

**Spin-coherent dynamics and carrier lifetime in strained  $\text{Ge}_{1-x}\text{Sn}_x$  semiconductors on silicon**S. De Cesari,<sup>1</sup> A. Balocchi,<sup>2,\*</sup> E. Vitiello,<sup>1</sup> P. Jahandar,<sup>3</sup> E. Grilli,<sup>1</sup> T. Amand,<sup>2</sup> X. Marie,<sup>2</sup> M. Myronov,<sup>3,†</sup> and F. Pezzoli<sup>1,‡</sup><sup>1</sup>*LNESS and Università degli Studi di Milano-Bicocca, via R. Cozzi 55, I-20125 Milano, Italy*<sup>2</sup>*Université de Toulouse, INSA-CNRS-UPS, LPCNO, 135 Ave. de Rangueil, 31077 Toulouse, France*<sup>3</sup>*Department of Physics, The University of Warwick, Coventry CV4 7AL, United Kingdom*

(Received 17 March 2018; revised manuscript received 21 December 2018; published 10 January 2019)

We demonstrate an effective epitaxial route for the manipulation and further enrichment of the intriguing spin-dependent phenomena boasted by germanium. We show optical initialization and readout of spins in Ge-rich germanium-tin alloys and report on spin quantum beats between Zeeman-split levels under an external magnetic field. While heavy Sn atoms can be readily utilized to strengthen the spin-orbit coupling, our experiments reveal robust spin orientation in a wide temperature range and a persistent spin lifetime that noticeably approaches the nanosecond regime at room temperature. In addition, time decay photoluminescence experiments evidence a temperature-induced monotonic decrease of the carrier lifetime, eventually providing crucial insights also into nonradiative recombination mechanisms.

DOI: [10.1103/PhysRevB.99.035202](https://doi.org/10.1103/PhysRevB.99.035202)**I. INTRODUCTION**

The outstanding challenge of overcoming fundamental limits of conventional device electronics has stimulated various proposals and extensive investigations of radical alternatives [1]. The prospect of utilizing quantum information and communication processing has placed group IV semiconductors at the leading edge of current research efforts [2–4]. Such materials are ubiquitous in the mainstream microelectronic industry and naturally exhibit favorable properties for the solid-state implementation of logic-gate operations built upon quantum states [5]. The centrosymmetric crystal structure and the essential abundance of spinless isotopes endow prominent group IV semiconductors, such as Si and Ge, with long-lived electron spins [2,6–8] exhibiting exceedingly long coherence times [9–11].

While Si lies ahead in the direction of quantum computation [12–14], Ge has a larger atomic number and sustains a stronger interaction between the spin and momentum degrees of freedom. Thanks to this property, Ge is emerging as a promising candidate for spin-to-charge conversion [15–17], eventually introducing the new route of spin-orbitronics [18] in the burgeoning field of group IV spintronics. The relativistic spin-orbit coupling (SOC) is also central to the intriguing spin-dependent phenomena potentially hosted by Ge, namely Majorana fermions [19] and Rashba states [7,16,20]. Notably, the spin-orbit interaction in conjunction with the quasidirect band structure of Ge leads to optimal coupling between spin states and light fields [21,22]. Such a key feature, unexpected in conventional indirect gap materials, has recently opened the way towards the optical exploration of a subtle electron spin dynamics [23–25], whose richness stems from the unique

multivalleyed structure of the conduction band of the material [26–28].

We expect that hybridizing the spin properties of Ge with the peculiar electronic states offered by  $\alpha$ -Sn, a heavier group IV element [29–31], can further enrich the spin-dependent phenomena hitherto observed in Ge. Alloying Ge with Sn can, in principle, introduce a novel degree of freedom to tailor the spin susceptibility to external fields, besides offering the key manipulation of spin electronic effects comprising novel quantum phases [32].

Despite such exciting prospects, the genuine potential of  $\text{Ge}_{1-x}\text{Sn}_x$  binary alloys remains presently unexplored. The main reason is that the large lattice mismatch and the low equilibrium solubility of Sn in Ge have impeded the direct large-scale deposition on Si wafers of high quality epitaxial heterostructures, especially at Sn-rich molar fractions [33]. Only very recent advances in out-of-equilibrium crystal growth techniques [33–36] have yielded reliable epitaxial films. However, even though lasing action has just been achieved at cryogenic temperatures [37–40], the fundamental understanding of carrier recombination mechanisms remains at an early stage, being jeopardized by fast and subtle nonradiative kinetic processes [37,41,42] and the often-impractical long-wavelength detection associated with the narrow band-gap transitions. Similarly, the spin properties of  $\text{Ge}_{1-x}\text{Sn}_x$  are still untapped, despite the noticeable demand of crucial data, like spin lifetimes, which is necessary for a critical advancement of the field.

Here we overcome the aforementioned limitations in an effort to address the spin dynamics and to refine the knowledge of the photonic properties of  $\text{Ge}_{1-x}\text{Sn}_x$ . To achieve this purpose, we gently break the inversion symmetry of the Ge lattice via substitutional Sn atoms to strengthen spin-orbit coupling, while preserving a desirably sizable spin lifetime. We thus focus on a Ge-rich  $\text{Ge}_{0.95}\text{Sn}_{0.05}$  epitaxial layer grown under compressive strain on a Ge-buffered Si substrate via state-of-the-art chemical vapor deposition [see Fig. 1(a)]. In

\*andrea.balocchi@insa-toulouse.fr

†m.myronov@warwick.ac.uk

‡fabio.pezzoli@unimib.it

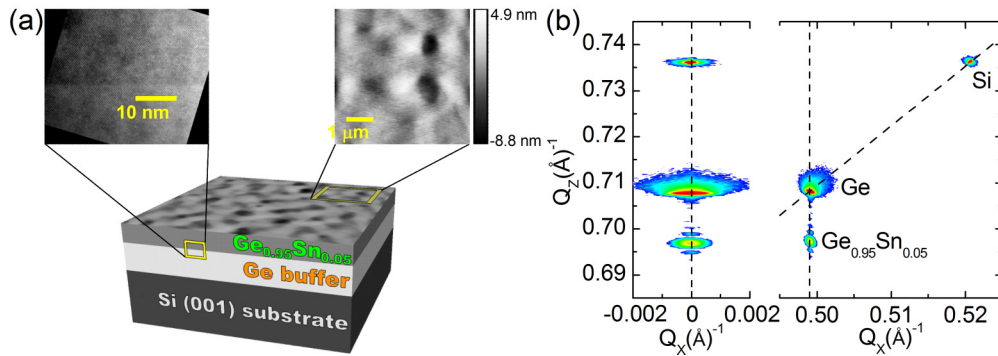


FIG. 1. (a) Sketch of the  $\text{Ge}_{0.95}\text{Sn}_{0.05}/\text{Ge}/\text{Si}$  heterostructure (not to scale). Cross-sectional transmission electron microscope image highlighting the GeSn/Ge heterointerface (left panel) and atomic force microscopy micrograph of the surface morphology of the sample (right panel). (b) X-ray diffraction (004) symmetric (left) and (224) asymmetric (right) reciprocal space maps. In the latter, the Bragg spots pertaining to Ge and GeSn are precisely aligned along the diffraction wave vector  $Q_x$  spanning the sample surface. This explicitly demonstrates the attained coherent growth condition. The Sn-based epilayer is indeed in perfect in-plane registry with the underlying Ge buffer.

this dilute alloy regime the strength of the SOC is expected to qualitatively mimic the one of well-established semiconductors like GaAs.

Moreover, thanks to pseudomorphic growth condition, we specifically inhibit the nucleation of detrimental crystal defects, mainly dislocations [42]. This is corroborated by an extensive structural characterization carried out throughout a broad array of techniques, including high-resolution x-ray diffraction (HR-XRD), transmission electron microscopy (TEM), and atomic force (AFM) microscopy (see Fig. 1).

The structural quality of the epitaxial stack spurs the challenge to directly probe carrier and spin-coherent dynamics by extending to longer wavelengths and shorter timescales the all-optical approach proved to be useful in elemental Ge. Time- and polarization-resolved photoluminescence (PL) experiments disclose in our Ge-rich  $\text{Ge}_{1-x}\text{Sn}_x$  heterostructure long-lived carrier and electron spin polarization up to room temperature. Remarkably, when we apply a magnetic field orthogonal to the spin polarization direction, we are able to observe, in a group IV semiconductor, the clear signature of spin quantum beats in the PL time decay [43,44]. This eventually unveils an effective electron  $g$  factor of about 1.5. Such findings enable us to scrutinize in detail the spin properties of  $\text{Ge}_{1-x}\text{Sn}_x$  and have the potential to stimulate the exploitation of new roads for basic research and advanced line of technologies based on these novel and intriguing alloys.

The paper is organized as follows. In Sec. II we discuss the experimental details of the investigation, while the carrier kinetics and the spin-dependent properties are reported in Secs. III and IV, respectively. Finally, Sec. V summarizes the results and the conclusions of this work.

## II. EXPERIMENTAL METHODS

The  $\text{Ge}_{1-x}\text{Sn}_x/\text{Ge}/\text{Si}(001)$  heterostructure was grown within a ASM Epsilon 2000 industrial type reduced pressure chemical vapor deposition (RP-CVD) system. A 70-nm-thick strained  $\text{Ge}_{1-x}\text{Sn}_x$  epilayer was deposited on a 100-mm-diameter Si (001) substrate via a relaxed Ge buffer with thickness  $\sim 650$  nm.  $\text{SnCl}_4$  was used as a Sn precursor, while

$\text{Ge}_2\text{H}_6$  was used as the Ge precursor. Growth was carried out at a temperature of  $280^\circ\text{C}$  in a  $\text{H}_2$  atmosphere. The sample has not been intentionally doped. We estimate the background doping to be below  $10^{15}\text{ cm}^{-3}$ .

A Jeol JEM-2100 TEM was used to obtain high-resolution cross-sectional micrographs of the heterostructure. TEM imaging allows direct observation of the crystalline quality and measurements of the epilayer's thickness. The surface morphology of the heterostructure was mapped using an Asylum Research MFP-3D stand-alone AFM operated in a tapping mode. The root mean square roughness turned out to be  $< 2$  nm. Finally, the Sn molar fraction of 5% and the biaxial compressive strain of 0.80% of the  $\text{Ge}_{1-x}\text{Sn}_x$  epilayer were measured from symmetrical (004) and asymmetrical (224) HR-XRD reciprocal space maps using a Panalytical X'Pert Pro MRD equipped with a  $\text{CuK}\alpha_1$  source.

Continuous-wave PL experiments were performed by exciting the sample with a Nd:YVO<sub>4</sub> laser at 1.165 eV. The spot diameter was about  $50\ \mu\text{m}$ , and the resulting power density was a few  $\text{kW}/\text{cm}^2$ . The polarized PL was dispersed by a monochromator coupled to a InGaAs photodiode detector with a cutoff at  $\sim 0.5$  eV. The spectra were numerically cleaned to remove the overlap with the second order peak of the pump. Time-resolved PL was carried out by using an excitation energy of 1.165 eV delivered by an optical parameter oscillator pumped by a Ti:Sa laser. The temporal width and the repetition rate of the laser pulses were  $\sim 2$  ps and 80 MHz, respectively. The laser spot size was estimated to be about  $7\ \mu\text{m}$  and the average excitation power was varied from 2.5 to 30 mW. The PL dynamics was determined by applying time-correlated single-photon counting using a superconducting nanowire detector with a time resolution of either 64 or 128 ps.

## III. CARRIER KINETICS IN PSEUDOMORPHIC $\text{Ge}_{1-x}\text{Sn}_x$ BINARY ALLOYS

### A. Low temperature PL and power dependence

The low-temperature PL, measured under continuous-wave excitation, demonstrates a prominent peak at about 0.64 eV [see Fig. 2(a)], which is attributed to band-to-band

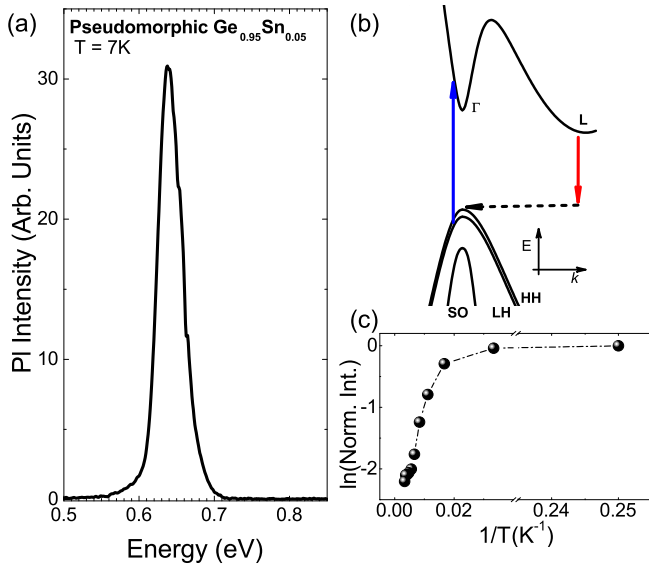


FIG. 2. (a) Low temperature PL spectrum of the Ge<sub>0.95</sub>Sn<sub>0.05</sub>/Ge/Si heterostructure measured at 7 K by utilizing a laser excitation energy of 1.165 eV. (b) Schematic representation of the energy ( $E$ ) band structure versus wave vector ( $k$ ) pertaining to a pseudomorphic Ge-rich Ge<sub>1-x</sub>Sn<sub>x</sub> epitaxial layer grown under compressive strain on a Ge-buffered Si substrate. Arrows show the low temperature absorption (blue) and emission (red) processes through the direct and indirect gap, respectively. (c) Temperature dependence of the spectrally integrated PL intensity.

transitions through the indirect gap of the Ge<sub>0.95</sub>Sn<sub>0.05</sub> epilayer as sketched in Fig. 2(b). Owing to the Sn molar fraction and compressive strain, the direct gap is expected to lie 100 meV higher in energy than the indirect gap [37,42], while the strain-induced splitting between heavy and light hole bands is of the order of 60 meV [45]. Emission from the buried Ge buffer is spectrally well separated [46] and is more than two orders of magnitude weaker than the one from the topmost Ge<sub>0.95</sub>Sn<sub>0.05</sub> film [42]. The PL intensity presented in Fig. 2(c) demonstrates a monotonic thermal-induced PL quenching, which is characterized by an activation energy of about 16 meV. As pointed out recently [42], this is a compelling spectroscopic fingerprint of the pseudomorphic nature of the Ge<sub>1-x</sub>Sn<sub>x</sub> layer. Such a distinct PL behavior would have been otherwise concealed by the presence of nonradiative recombination channels opened up by dislocations. Such extended defects are introduced in the Ge<sub>1-x</sub>Sn<sub>x</sub> epitaxial layers through plastic strain relaxation and are known to trigger a Schon-Klasens-like recombination dynamics, which enhances the PL intensity in the high temperature regime [42,46–48].

Figure 3 reports low-temperature PL intensity dynamics measured at various pump fluencies. A non-monoexponential decay time is observed. We start by considering the low excitation, i.e., an average excitation power  $P_{AV} = 2.5$  mW (black line in Fig. 3). Under such conditions, the early phase of the recombination process exhibits a rather slow decay, which becomes steeper during the later stage of the temporal evolution (after 4 ns). This puzzling PL transient can be accounted for by considering two intertwined recombination mechanisms. The fastest component of the decay curve

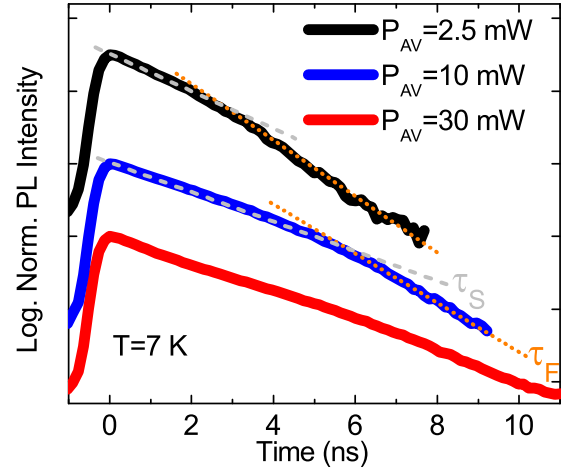


FIG. 3. Low-temperature normalized PL dynamics of the pseudomorphic Ge<sub>0.95</sub>Sn<sub>0.05</sub> epitaxial layer as a function of the average excitation power. The pump pulse has an energy of  $\approx 1.165$  eV and a duration of about 2 ps. Decay curves have been vertically shifted for clarity. The straight lines are guides to the eye for pointing out the fast ( $\tau_F$ ) and slow ( $\tau_S$ ) decay components.

suggests a large recombination probability controlled by an efficient nonradiative recombination channel. Its influence on the carrier kinetics is however masked during the slower initial decay phase. Knowing that the PL transient mimics the time evolution of the photoexcited population, we can conclude that the likely culprit for the initially diminished decay rate is the density of the excess carriers. At first, the pump pulse generates a large density of carriers that quite quickly saturates the low-energy states available for the fast recombination process. This leads to the observation of a less efficient recombination pathway characterized by a slower characteristic time. Later, the depopulation of the nonradiative centers activates the competing channel, whose effectiveness drastically accelerates the temporal decay of the PL.

The accuracy of this interpretation is further corroborated by the excitation intensity curves of Fig. 3, which shows that a decreased pump power advances the change in slope of the decay curve, thus making the slow component less relevant for reduced densities of the photoexcited carriers. A similar behavior can be consistently observed by increasing the lattice temperature (not shown).

## B. Temperature dependence and modeling of the recombination processes

After having unveiled the occurrence of nonradiative recombination pathways, we focus on the analysis of the temperature-induced PL characteristic to gather a better understanding of all the kinetic processes.

Figure 4 summarizes the carrier lifetimes derived from the two slopes of the PL decay curves measured at various lattice temperatures. In this case, we have carried out the measurements at a fixed intermediate pump power, i.e.,  $P_{AV} = 10$  mW, in order to be able to better appreciate the slower ( $\tau_S$ ) and faster ( $\tau_F$ ) decay components over a large temperature range. Our experiments unveil that the PL dynamics occurs within a couple of nanoseconds and is faster in the high

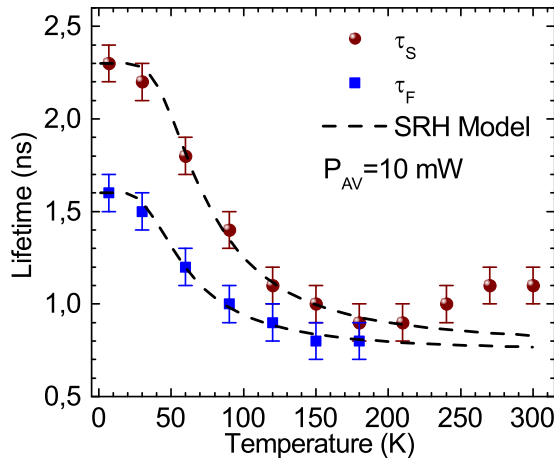


FIG. 4. The red (blue) dots represent the slow ( $\tau_S$ ) and fast ( $\tau_F$ ) components of the PL decay curves. All the experimental data have been obtained by using an average excitation power of  $P_{AV} = 10$  mW. The black dashed curves are modeled according to the Shockley-Read-Hall (SRH) statistics pertaining to the recombination processes.

temperature regime. Since the band-to-band recombination pertaining to indirect gap materials is expected to develop on a slower timescale [8,47], we attribute the measured temperature dependence of the lifetime to the presence of extrinsic recombination channels defined by shallow energy levels.

The temperature characteristic of the carrier lifetime stems from the dependence of the carrier density upon the temperature and is akin to the qualitative behavior inferred by the steady-state PL in direct band-gap  $\text{Ge}_{1-x}\text{Sn}_x$  layers [37]. The latter are indeed characterized by a monotonic temperature-induced PL quenching similar to the one observed in this work [see Fig. 2(c)]. In particular, the data of Fig. 4 demonstrate that  $\tau_S$  approaches the flatter temperature response of  $\tau_F$  at about 180 K: the temperature above which the two components can no longer be distinguished. By further increasing the temperature, the carrier lifetime notably reaches a minimum and above 210 K demonstrates an unexpected, albeit modest, lengthening.

The temperature-induced changes of the carrier lifetime in  $\text{Ge}_{1-x}\text{Sn}_x$  can be modeled by using the recombination statistics [49–51] and by assuming the presence of energy states lying within the forbidden gap. According to such a physical picture, a photogenerated carrier can be effectively captured by traps that provide nonradiative recombination pathways.

The total carrier lifetime  $\tau$  can indeed be described as  $1/\tau = 1/\tau_r + 1/\tau_{nr}$ , where the total nonradiative lifetime  $\tau_{nr}$  can be conveniently decomposed into Auger- and trap-limited lifetimes, respectively  $\tau_{Auger}$  and  $\tau_{SRH}$ , as  $1/\tau_{nr} = 1/\tau_{Auger} + 1/\tau_{SRH}$ . We notice that our power-dependent PL decay data do not show the typical features of Auger recombination, namely an initial fast decay time that is dependent upon the excess-carrier density [8]. In addition, at cryogenic temperatures the measured decay times in our Ge-rich  $\text{Ge}_{1-x}\text{Sn}_x$  sample are shorter than 2 ns, whereas the typical Auger lifetimes in Ge are in the regime of few tens of nanoseconds [8,42]. As a

result, we can neglect the first term on the right-hand side of the above-mentioned equation and focus our attention on the Shockley-Read-Hall recombination given by traps, whose temperature dependence in a not intentionally doped sample reads  $\tau_{SRH} = \tau_0[1 + \cosh \Delta E/(k_B T)]$  [37,49,50]. Here  $\Delta E$  is the energy difference between the trap and the intrinsic Fermi level, while  $\tau_0^{-1}$  provides the rate of captures of minority carriers by the defects. The experimental data of the carrier lifetime for the fast and slow decay components of pseudomorphic  $\text{Ge}_{1-x}\text{Sn}_x$  have thus been modeled within the SRH framework.

The excellent agreement between the calculation and the experimental data, uncovered in the low and intermediate temperature regimes by Fig. 4, reveals that the fast (slow) decay component is well described by a nonradiative trap that resides at about 13 meV ( $\sim 17$  meV) above the Fermi level. Such energy compares satisfactorily with a temperature of 150 K, above which the fast decay turns out to be washed out.

It is illuminating to note that the SRH formalism ascribes the slower  $\tau_S$  component to the presence of a second shallower trap. This is strikingly in line with the conclusions of the power-dependent analysis summarized in Fig. 3. The possible occurrence of thermal-induced quenching of this defect state is expected to occur for a thermal energy that corresponds to a temperature of about 200 K. According to Fig. 4 such value marks an increase in the carrier lifetime. This makes a strong case for a partial suppression of this second trap and a concomitant emergence of recombination processes that lengthen the near-room-temperature kinetics of the carriers. This finding eventually clarifies the apparent discrepancy arising in the high temperature regime between the experimental data and the modeling based on the two component SRH dynamics.

## IV. SPIN-DEPENDENT PROPERTIES

### A. Optical spin orientation

Besides corroborating the structural characterization of the sample, the optical properties of the pseudomorphic layer allow us to perform optical orientation experiments [52–54] to verify the possibility of generating an out-of-equilibrium ensemble of spins directly in the  $\text{Ge}_{1-x}\text{Sn}_x$  layer by optical means. In Fig. 5 we observe that, upon excitation with a continuous-wave  $\sigma^+$  polarized laser, there is an imbalance between the right- ( $I^{\sigma^+}$ ) and left- ( $I^{\sigma^-}$ ) circularly polarized components of the PL. We also notice that the circular PL polarization degree, hereby defined under steady state conditions as  $\rho_{circ} = \frac{I^{\sigma^+} - I^{\sigma^-}}{I^{\sigma^+} + I^{\sigma^-}}$ , is robust over a wide temperature range. Remarkably,  $\rho_{circ}$  turns out to be sizable even at room temperature, although smaller than the 25% expected in a relaxed bulk system [52,54].

The measured  $\rho_{circ}$  at steady state is linked to the carrier lifetime  $\tau$  and the spin relaxation  $T_1$  via the following equation:  $\rho_{circ} = \rho_0(1 + \tau/T_1)$ , in which  $\rho_0$  is the polarization in absence of relaxation mechanisms [52]. The latter endows fundamental information about the band structure of the material [52,54]. Due to the lack of theoretical and experimental data to guide the interpretation of optical injection

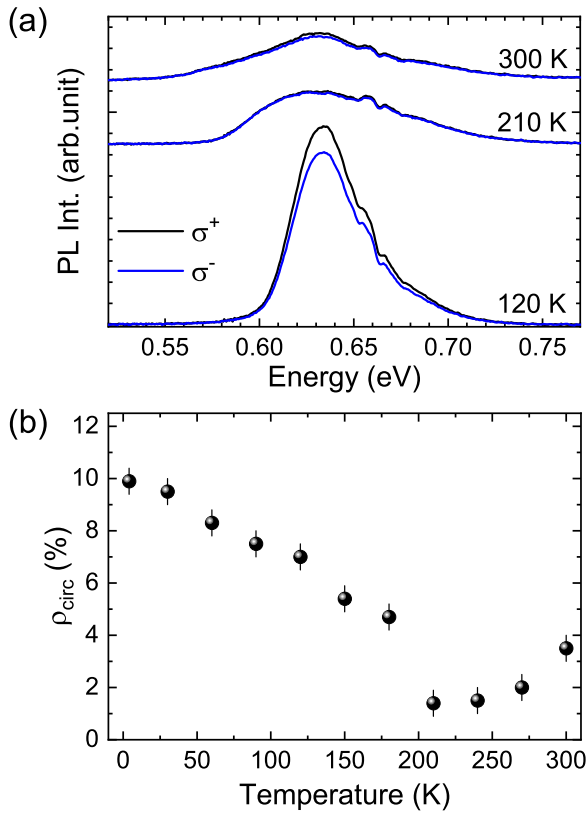


FIG. 5. (a) PL spectra for the Ge<sub>0.95</sub>Sn<sub>0.05</sub>/Ge/Si heterostructure measured at 120, 210, and 300 K for right- and left-handed circular polarizations, namely  $\sigma^+$  (black curve) and  $\sigma^-$  (blue curve), respectively. The spectra have been vertically shifted for clarity. (b) Temperature dependence of the circular polarization degree ( $\rho_{\text{circ}}$ ) measured under steady state conditions.

experiments of spin-polarized carriers in Ge<sub>1-x</sub>Sn<sub>x</sub>, we shall rely on the knowledge of closely related semiconductors, such as Ge and GaAs, to interpret the results summarized in Fig. 5(b). We can thus speculate that the observed polarization degree stems from the excitation energy of our pump, which leads to absorption from split-off band and to a concomitant reduced polarization of electrons optically coupled to light hole states [55].

The findings shown in Fig. 5, along with the expected fast spin relaxation of holes [56,57], unambiguously demonstrate the successful optical generation of a net spin polarization of electrons in the conduction band of Ge<sub>1-x</sub>Sn<sub>x</sub>. Additionally, these results point towards non-negligible electron spin relaxation times.

### B. Dependence of spin relaxation time upon carrier density and temperature

In the following we apply optical spectroscopy in the time domain to explore the kinetics and to gather a better understanding of the anticipated spin properties. Figure 6(a) demonstrates different intensities for the helicity-resolved PL transient following a circularly polarized excitation laser. This imbalance further corroborates the successful achievement of optical spin orientation of electrons in the Ge<sub>1-x</sub>Sn<sub>x</sub>

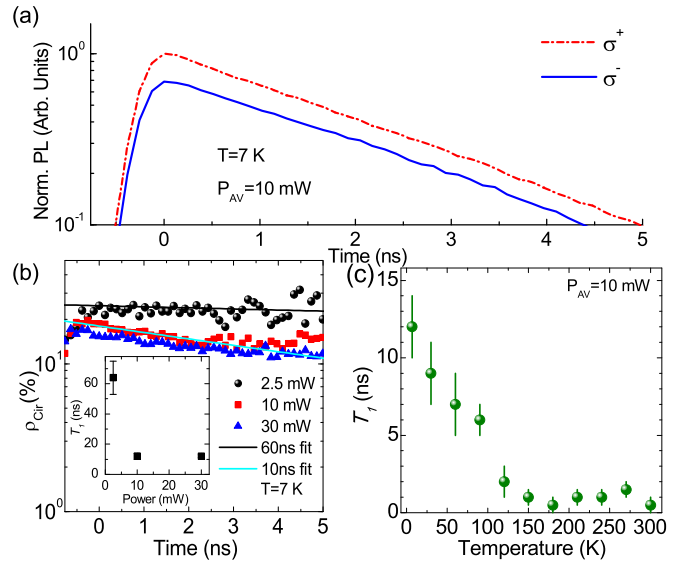


FIG. 6. (a) Temporal evolution of the polarization-resolved PL of Ge<sub>0.95</sub>Sn<sub>0.05</sub> at an average pump power  $P_{\text{AV}}$  of 10 mW and a lattice temperature of 7 K. Right-handed circular polarization ( $\sigma^+$ ) is shown as a dashed red line, whereas the left-handed helicity ( $\sigma^-$ ) is reported as a blue line (the excitation laser is  $\sigma^+$  polarized). (b) Low-temperature decay dynamics of the circular polarization degree  $\rho_{\text{circ}}$ . Black dots, red squares, and blue triangles refer to an average pump power equal to 2.5, 10, and 30 mW, respectively. The black (blue) line is a fit of the low (high) power decay curve which provides a decay time of 60 (10) ns. The inset demonstrates the derived spin relaxation time  $T_1$  as a function of the excitation power. (c) Temperature dependence of  $T_1$  for  $P_{\text{AV}} = 10$  mW.

conduction band. In Fig. 6(a) it can also be noted that the two polarization-resolved decay curves are almost parallel. This indicates a rather long spin relaxation time, which in the low power limit and for a dilute Sn alloy as in the present case, is ultimately expected to be governed by the Elliot-Yafet mechanism [26].

The spin relaxation time can be directly obtained by the decay time of  $\rho_{\text{circ}}$  derived from the PL data. Figure 6(b) reveals that the pump drastically affects the spin dynamics, since the decay rate of the polarization degree strikingly increases with the laser power density. A variation in the average excitation power from 30 to 2.5 mW lengthens the spin relaxation time from about 10 to 60 ns [see the inset of Fig. 6(b)]. Although the longest value must be solely regarded as an upper limit, being retrieved from a much shorter transient time, the observed power dependence of  $T_1$  points towards the occurrence of optically induced spin-flip processes and suggests the importance of electron-hole Coulomb exchange interaction among the out-of-equilibrium spin ensemble [7,52,58].

This finding is further supported by a systematic investigation of the spin lifetime as a function of the temperature. Figure 6(c) shows that  $T_1$  steadily decreases as the temperature is increased from 7 to 200 K. Interestingly,  $T_1$  remains rather constant at higher temperatures. The following scenario likely accounts for such observations. At low temperatures, the electron spin relaxation is dominated, under our

TABLE I. Spin dependent parameters of relevant semiconductors. The spin-orbit splitting  $\Delta_{SO}$  can be utilized to provide a qualitative metrics for the strength of spin-orbit coupling in a given material. The spin relaxation times at room temperature are reported in the last column.

	$\Delta_{SO}$ (meV)	$T_1$ (ns) at 300 K
Si	44	6 [61], 8 [62]
Ge	290	1 [26], 0.5 [63], 0.25 [64,65]
Ge <sub>0.95</sub> Sn <sub>0.05</sub>	320 [45]	0.5
GaAs	350	<0.9 [66,67]

experimental conditions, by exchange interaction with photoinduced holes. In this temperature regime, the optical activity of the defect states, being largely occupied by extrinsic carriers, turns out to be mitigated. Thermal-induced ionization of the shallow traps, however, activates nonradiative recombination events that shorten the carrier lifetime and eventually increases the concentration of unpolarized free carriers. The latter can contribute along with scattering off the central-cell potential of the impurities [59] and the phonon mediated spin-flip processes [26,60] to the temperature-driven Elliot-Yafet spin relaxation observed in Fig. 6(c).

It should be noted that  $T_1$  remains in the nanosecond regime even in the high temperature range and approaches the values expected in elemental Ge [26,60]. Table I specifically summarizes a more direct comparison with some of

the available values of the spin lifetime reported at room temperature for bulk Ge and other prominent semiconductors. Our findings suggest that the small amount of the heavier element Sn, incorporated in the lattice, gently perturbs the electron spin properties, thus preserving (i) the favorable spin-orbit coupling pertaining to the Ge band structure and (ii) an almost perfect  $O_h$  symmetry of the lattice, so that Dyakonov-Perel relaxation is not significant. The former property has been remarkably identified as a key feature that enables Ge to support exceedingly long spin lifetimes [7,26].

In light of these considerations, we expect that alloying Ge with Sn can offer a novel degree of freedom to engineer phenomena based on spin-orbit coupling, such as Rashba or spin Hall effects, while retaining a desirably long spin relaxation. Finally, we notice that the  $T_1$  regime measured at room temperature is already comparable to the typical switching frequency of standard electronic devices, thus increasing the prospects of a practical implementation of Ge<sub>1-x</sub>Sn<sub>x</sub> for spin transport and manipulation in future device architectures.

### C. Quantum beat spectroscopy and coherent spin dynamics

In the following we extend our all-optical investigation by measuring the electron spin dynamics under the presence of an external magnetic field ( $B$ ) in Voigt geometry, e.g.,  $B \parallel [110]$ . In particular, we apply spin quantum beat spectroscopy to Ge-based systems, demonstrating coherent spin dynamics and providing an estimation of the Landé  $g$  factor of conduction electrons in strained Ge<sub>1-x</sub>Sn<sub>x</sub> layers.

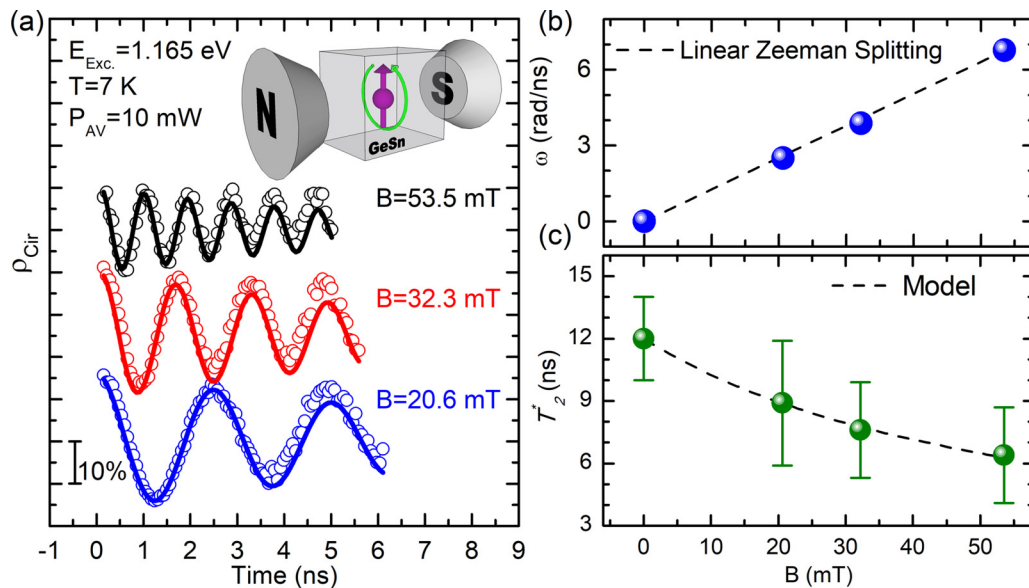


FIG. 7. (a) Magnetic field dependence of the dynamics of the circular polarization degree ( $\rho_{\text{circ}}$ ) measured at a lattice temperature of 7 K and for a laser excitation energy of 1.165 eV and  $P_{AV} = 10$  mW. Experimental data obtained by applying a magnetic field strength of 20.6 (blue dots), 32.3 (red dots), and 53.5 mT (black dots) and the corresponding fits (solid lines) have been shifted for clarity.  $\rho_{\text{circ}}$  oscillates around zero and the quantum beatings can be interpreted in terms of the Larmor precession of the electron spins due to the presence of an external magnetic field perpendicular to the quantization axis (Voigt configuration, see inset). (b) Dependence of the Larmor frequency  $\omega$  on the magnetic field strength for a fully strained Ge<sub>0.95</sub>Sn<sub>0.05</sub> layer epitaxially deposited on a Ge buffered Si substrate. The dashed line corresponds to the linear dependence determined by the Zeeman splitting  $\hbar\omega = g^*\mu_B B$ , where  $g^*$  is the effective  $g$  factor and  $\mu_B$  is the Bohr's magneton. (c) Ensemble spin coherence time  $T_2^*$  as a function of the external magnetic field strength. Experimental data have been obtained by the magnetic field dependence of the damping of the quantum beats. The dashed line in the figure is based on a modeling that correlates the spin dephasing time and the microscopic  $g$  factor spread in the alloy layer.

The intensity oscillations of the PL circular polarization displayed in Fig. 7(a) reflect the Larmor precession of the electron spins in the transverse magnetic field. The precession frequency  $\omega$  depends on the strength of the magnetic field as  $\hbar\omega = g^*\mu_B B$ , where  $\mu_B$  is the Bohr's magneton and  $g^*$  is the effective  $g$  factor. Figures 7(a) and 7(b) nicely demonstrate such a linear relationship and allow us to determine the effective Landé factor of conduction electrons. We find  $g^* = 1.48 \pm 0.01$ . This value compares favorably with recent reports of the Landé  $g$  factor of  $L$ -valleys electrons in Ge [7,68].

While previous works on Ge resolved multiple  $g$ -factor values disclosing a large anisotropy [7,68], our findings suggest for GeSn one precession frequency, that is, a single effective  $g$  factor. We can start considering that Fig. 7 shows the only data available in the literature that have been derived from PL of group IV materials. In a PL experiment, the optical excitation generates spin-polarized electrons with a relatively large excess energy with respect to the conduction band edge. The energy relaxation process of such hot electrons is likely to occur via intervalley rather than intravalley scattering. The latter is expected however to dominate the dynamics of thermal electrons at cryogenic temperatures. The  $g$ -factor anisotropy might be thus washed out for the optically injected carriers, eventually yielding a single PL transient as observed in Fig. 7. This mechanisms can have important consequences also on the spin relaxation. Optical excitation can activate the intervalley spin relaxation channel even at temperatures at which such scattering mechanisms should be inhibited because of the negligible population of zone-edge phonons [26].

We observe in Fig. 7 that the magnetic field amplitude affects the period of the quantum beats along with their damping time. The latter feature, summarized in Fig. 7(c), discloses the presence of transverse spin relaxation mechanisms. The substantial decrease of the dephasing time of the spin ensemble ( $T_2^*$ ) with the strength of applied magnetic field is a result of  $g$ -factor fluctuations,  $\Delta g$  [69,70]. Indeed, in the optical orientation process, light absorption

generates conduction electrons with a finite excess energy. Spin dephasing is triggered by the cooling process, during which electrons experience momentum relaxation and random effective magnetic fields given by local changes in the alloy composition and strain. Data in Fig. 7(c) are well described by the equation [70]  $1/T_2^*(B) = 1/T_2^*(0) + \Delta g\mu_B B/\hbar$  (black line) resulting from a normal distribution of  $g$  factors, and provides us with a  $\Delta g$  of  $2.1 \times 10^{-2}$ .

## V. CONCLUSIONS

The measurement of the PL decay curves allowed us to gather insights into recombination mechanisms and to resolve the physics of carrier dynamics over a wide temperature range. These findings can be utilized in the quest for achieving real-life deployment of light emitting devices based on  $\text{Ge}_{1-x}\text{Sn}_x$  alloys. Furthermore, we have explored the exciting prospect of utilizing a new group IV material, such as  $\text{Ge}_{1-x}\text{Sn}_x$ , as future solid-state hosts of spin-based information. The tunable band structure and SOC, promised by this novel alloy, can potentially offer a very rich spin physics, whose fundamental understanding is however still absent. The demonstrated applicability of light-matter interaction facilitated in this work the anticipation of spin-dependent phenomena pertaining to this notable material. Robust quantum coherence within a spin ensemble has been observed and loss mechanisms induced by local alloy fluctuations identified. Finally, the PL dynamics measurements allowed us to gather insights into the spin dynamics over a wide temperature range. Looking ahead, the determination of the effective Landé  $g$  factor and the temperature-dependent spin-flip mechanisms can provide key information for the future design of spintronic devices and the potential applicability of  $\text{Ge}_{1-x}\text{Sn}_x$  for gate-defined spin qubits.

## ACKNOWLEDGMENTS

X.M. acknowledges Institut Universitaire de France. This work was supported by Fondazione CARIPLO through the project SEARCH-IV, Grant No. 2013-0623.

- 
- [1] M. M. Waldrop, The chips are down for Moore's law, *Nature (London)* **530**, 144 (2016).
  - [2] J. J. L. Morton, D. R. McCamey, M. A. Eriksson, and S. A. Lyon, Embracing the quantum limit in silicon computing, *Nature (London)* **479**, 345 (2011).
  - [3] R. Jansen, Silicon spintronics, *Nat. Mater.* **11**, 400 (2012).
  - [4] C. Morrison and M. Myronov, Strained germanium for applications in spintronics, *Phys. Status Solidi A* **213**, 2809 (2016).
  - [5] F. A. Zwanenburg, A. S. Dzurak, A. Morello, M. Y. Simmons, L. C. L. Hollenberg, G. Klimeck, S. Rogge, S. N. Coppersmith, and M. A. Eriksson, Silicon quantum electronics, *Rev. Mod. Phys.* **85**, 961 (2013).
  - [6] P. Li and H. Dery, Spin-Orbit Symmetries of Conduction Electrons in Silicon, *Phys. Rev. Lett.* **107**, 107203 (2011).
  - [7] A. Giorgioni, S. Paleari, S. Cecchi, E. Vitiello, E. Grilli, G. Isella, W. Jantsch, M. Fanciulli, and F. Pezzoli, Strong confinement-induced engineering of the  $g$  factor and lifetime of conduction electron spins in Ge quantum wells, *Nat. Commun.* **7**, 13886 (2016).
  - [8] A. Giorgioni, E. Vitiello, E. Grilli, M. Guzzi, and F. Pezzoli, Valley-dependent spin polarization and long-lived electron spins in germanium, *Appl. Phys. Lett.* **105**, 152404 (2014).
  - [9] A. M. Tyryshkin, S. Tojo, J. J. L. Morton, H. Riemann, N. V. Abrosimov, P. Becker, H. J. Pohl, M. L. W. Schenkel, T. Thewalt, K. M. Itoh, and S. A. Lyon, Electron spin coherence exceeding seconds in high-purity silicon, *Nat. Mater.* **11**, 143 (2012).
  - [10] A. J. Sigillito, R. M. Jock, A. M. Tyryshkin, J. W. Beeman, E. E. Haller, K. M. Itoh, and S. A. Lyon, Electron Spin Coherence of Shallow Donors in Natural and Isotopically Enriched Germanium, *Phys. Rev. Lett.* **115**, 247601 (2015).
  - [11] J. T. Muhonen, J. P. Dehollain, A. Laucht, F. E. Hudson, R. Kalra, T. Sekiguchi, K. M. Itoh, D. N. Jamieson,

- J. C. McCallum, A. S. Dzurak, and A. Morello, Storing quantum information for 30 seconds in a nanoelectronic device, *Nat. Nanotechnol.* **9**, 986 (2014).
- [12] J. J. Pla, K. Y. Tan, J. P. Dehollain, W. H. Lim, J. J. L. Morton, D. N. Jamieson, A. S. Dzurak, and A. Morello, A single-atom electron spin qubit in silicon, *Nature (London)* **489**, 541 (2012).
- [13] R. Maurand, X. Jehl, D. Kotekar-Patil, A. Corna, H. Bohuslavskiy, R. Lavieville, L. Hutin, S. Barraud, M. Vinet, M. Sanquer, and S. De Franceschi, A CMOS silicon spin qubit, *Nat. Commun.* **7**, 13575 (2016).
- [14] T. F. Watson, S. G. J. Philips, E. Kawakami, D. R. Ward, P. Scarlino, M. Veldhorst, D. E. Savage, M. G. Lagally, M. Friesen, S. N. Coppersmith, M. A. Eriksson, and L. M. K. Vandersypen, A programmable two-qubit quantum processor in silicon, *Nature (London)* **555**, 633 (2018).
- [15] S. Dushenko, M. Koike, Y. Ando, T. Shinjo, M. Myronov, and M. Shiraishi, Experimental Demonstration of Room-Temperature Spin Transport in *n*-Type Germanium Epilayers, *Phys. Rev. Lett.* **114**, 196602 (2015).
- [16] S. Oyarzün, A. K. Nandy, F. Rortais, J.-C. Rojas-Sanchez, M.-T. Dau, P. Noël, P. Laczkowski, S. Pouget, H. Okuno, L. Vila, C. Vergnaud, C. Beigné, A. Marty, J.-P. Attané, S. Gambarelli, J.-M. George, H. Jaffrès, S. Blügel, and M. Jamet, Evidence for spin-to-charge conversion by Rashba coupling in metallic states at the Fe/Ge(111) interface, *Nat. Commun.* **7**, 13857 (2016).
- [17] F. Bottegoni, C. Zucchetti, S. Dal Conte, J. Frigerio, E. Carpena, C. Vergnaud, M. Jamet, G. Isella, F. Ciccacci, G. Cerullo, and M. Finazzi, Spin-Hall Voltage Over a Large Length Scale in Bulk Germanium, *Phys. Rev. Lett.* **118**, 167402 (2017).
- [18] A. Hoffmann and S. D. Bader, Opportunities at the frontiers of spintronics, *Phys. Rev. Appl.* **4**, 047001 (2015).
- [19] F. Maier, J. Klinovaja, and D. Loss, Majorana fermions in Ge/Si hole nanowires, *Phys. Rev. B* **90**, 195421 (2014).
- [20] R. Moriya, K. Sawano, Y. Hoshi, S. Masubuchi, Y. Shiraki, A. Wild, C. Neumann, G. Abstreiter, D. Bougeard, T. Koga, and T. Machida, Cubic Rashba Spin-Orbit Interaction of a Two-Dimensional Hole Gas in a Strained-Ge/SiGe Quantum Well, *Phys. Rev. Lett.* **113**, 086601 (2014).
- [21] R. Allenspach, F. Meier, and D. Pescia, Experimental Symmetry Analysis of Electronic States by Spin-Dependent Photoemission, *Phys. Rev. Lett.* **51**, 2148 (1983).
- [22] F. Pezzoli, A. Balocchi, E. Vitiello, T. Amand, and X. Marie, Optical orientation of electron spins and valence-band spectroscopy in germanium, *Phys. Rev. B* **91**, 201201(R) (2015).
- [23] E. J. Loren, B. A. Ruzicka, L. K. Werake, H. Zhao, H. M. van Driel, and A. L. Smirl, Optical injection and detection of ballistic pure spin currents in Ge, *Appl. Phys. Lett.* **95**, 092107 (2009).
- [24] C. Guite and V. Venkataraman, Measurement of Electron Spin Lifetime and Optical Orientation Efficiency in Germanium using Electrical Detection of Radio Frequency Modulated Spin Polarization, *Phys. Rev. Lett.* **107**, 166603 (2011).
- [25] F. Pezzoli, F. Bottegoni, D. Trivedi, F. Ciccacci, A. Giorgioni, P. Li, S. Cecchi, E. Grilli, Y. Song, M. Guzzi, H. Dery, and G. Isella, Optical Spin Injection and Spin Lifetime in Ge Heterostructures, *Phys. Rev. Lett.* **108**, 156603 (2012).
- [26] P. Li, Y. Song, and H. Dery, Intrinsic spin lifetime of conduction electrons in germanium, *Phys. Rev. B* **86**, 085202 (2012).
- [27] F. Pezzoli, L. Qing, A. Giorgioni, G. Isella, E. Grilli, M. Guzzi, and H. Dery, Spin and energy relaxation in germanium studied by spin-polarized direct-gap photoluminescence, *Phys. Rev. B* **88**, 045204 (2013).
- [28] A. Giorgioni, F. Pezzoli, E. Gatti, S. Cecchi, C. K. Inoki, C. Deneke, E. Grilli, G. Isella, and M. Guzzi, Optical tailoring of carrier spin polarization in Ge/SiGe multiple quantum wells, *Appl. Phys. Lett.* **102**, 012408 (2013).
- [29] A. Barfuss, L. Dudy, M. R. Scholz, H. Roth, P. Hopfner, C. Blumenstein, G. Landolt, J. H. Dil, N. C. Plumb, M. Radovic, A. Bostwick, E. Rotenberg, A. Fleszar, G. Bihlmayer, D. Wortmann, G. Li, W. Hanke, R. Claessen, and J. Schafer, Elemental Topological Insulator with Tunable Fermi Level: Strained  $\alpha$ -Sn on InSb(001), *Phys. Rev. Lett.* **111**, 157205 (2013).
- [30] Y. Ohtsubo, P. Le Fevre, F. Bertran, and A. Taleb-Ibrahimi, Dirac Cone with Helical Spin Polarization in Ultrathin  $\alpha$ -Sn(001) Films, *Phys. Rev. Lett.* **111**, 216401 (2013).
- [31] C. Z. Xu, Y. H. Chan, Y. G. Chen, P. Chen, X. X. Wang, C. Dejoie, M. H. Wong, J. A. Hlevyack, H. J. Ryu, H. Y. Kee, N. Tamura, M. Y. Chou, Z. Hussain, S. K. Mo, and T. C. Chiang, Elemental Topological Dirac Semimetal:  $\alpha$ -Sn on InSb(111), *Phys. Rev. Lett.* **118**, 146402 (2017).
- [32] H. S. Lan, S. T. Chang, and C. W. Liu, Semiconductor, topological semimetal, indirect semimetal, and topological Dirac semimetal phases of  $\text{Ge}_{1-x}\text{Sn}_x$  alloys, *Phys. Rev. B* **95**, 201201(R) (2017).
- [33] S. Wirths, D. Buca, and S. Mantl, Si-Ge-Sn alloys: From growth to applications, *Prog. Cryst. Growth* **62**, 1 (2016).
- [34] V. R. D'Costa, Y. Y. Fang, J. Tolle, J. Kouvetakis, and J. Menéndez, Tunable Optical Gap at a Fixed Lattice Constant in Group-IV Semiconductor Alloys, *Phys. Rev. Lett.* **102**, 107403 (2009).
- [35] B. Vincent, F. Gencarelli, H. Bender, C. Merckling, B. Douhard, D. H. Petersen, O. Hansen, H. H. Henrichsen, J. Meererschaut, W. Vandervorst, M. Heyns, R. Loo, and M. Caymax, Undoped and in-situ B doped GeSn epitaxial growth on Ge by atmospheric pressure-chemical vapor deposition, *Appl. Phys. Lett.* **99**, 152103 (2011).
- [36] M. Bauer, C. Ritter, P. A. Crozier, J. Ren, J. Menéndez, G. Wolf, and J. Kouvetakis, Synthesis of ternary SiGeSn semiconductors on Si(100) via  $\text{Sn}_x\text{Ge}_{1-x}$  buffer layers, *Appl. Phys. Lett.* **83**, 2163 (2003).
- [37] S. Wirths, R. Geiger, N. von den Driesch, G. Mussler, T. Stoica, S. Mantl, Z. Ikonc, M. Luysberg, S. Chiussi, J. M. Hartmann, H. Sigg, J. Faist, D. Buca, and D. Grützmacher, Lasing in direct-bandgap GeSn alloy grown on Si, *Nat. Photon.* **9**, 88 (2015).
- [38] S. Al-Kabi, S. A. Ghetmiri, J. Margetis, T. Pham, Y. Zhou, W. Dou, B. Collier, R. Quinde, W. Du, A. Mosleh, J. Liu, G. Sun, R. A. Soref, J. Tolle, B. Li, M. Mortazavi, H. A. Naseem, and S. Q. Yu, An optically pumped 2.5  $\mu\text{m}$  GeSn laser on Si operating at 110 K, *Appl. Phys. Lett.* **109**, 171105 (2016).
- [39] V. Reboud, A. Gassenq, N. Pauc, J. Aubin, L. Milord, Q. M. Thai, M. Bertrand, K. Guilloy, D. Rouchon, J. Rothman, T. Zabel, F. Armand Pilon, H. Sigg, A. Chelnokov, J. M. Hartmann, and V. Calvo, Optically pumped GeSn micro-disks with 16% Sn lasing at 3.1  $\mu\text{m}$  up to 180 K, *Appl. Phys. Lett.* **111**, 092101 (2017).
- [40] J. Margetis, S. Al-Kabi, W. Du, W. Dou, Y. Zhou, T. Pham, P. Grant, S. Ghetmiri, A. Mosleh, B. Li, J. Liu, G. Sun, R. Soref,

- J. Tolle, M. Mortazavi, and S.-Q. Yu, Si-based GeSn lasers with wavelength coverage of 2–3  $\mu\text{m}$  and operating temperatures up to 180 K, *ACS Photon.* **5**, 827 (2018).
- [41] J. D. Gallagher, C. L. Senaratne, C. Xu, P. Sims, T. Aoki, D. J. Smith, J. Menéndez, and J. Kouvetakis, Non-radiative recombination in  $\text{Ge}_{1-y}\text{Sn}_y$  light emitting diodes: The role of strain relaxation in tuned heterostructure designs, *J. Appl. Phys.* **117**, 245704 (2015).
- [42] F. Pezzoli, A. Giorgioni, D. Patchett, and M. Myronov, Temperature-dependent photoluminescence characteristics of GeSn epitaxial layers, *ACS Photon.* **3**, 2004 (2016).
- [43] T. Amand, X. Marie, P. LeJeune, M. Brousseau, D. Robart, J. Barrau, and R. Planel, Spin Quantum Beats of 2D Excitons, *Phys. Rev. Lett.* **78**, 1355 (1997).
- [44] A. P. Heberle, W. W. Ruhle, and K. Ploog, Quantum Beats of Electron Larmor Precession in GaAs Wells, *Phys. Rev. Lett.* **72**, 3887 (1994).
- [45] K. Zelazna, M. P. Polak, P. Scharoch, J. Serafinczuk, M. Gladysiewicz, J. Misiewicz, J. Dekoster, and R. Kudrawiec, Electronic band structure of compressively strained  $\text{Ge}_{1-x}\text{Sn}_x$  with  $x < 0.11$  studied by contactless electroreflectance, *Appl. Phys. Lett.* **106**, 142102 (2015).
- [46] F. Pezzoli, F. Isa, G. Isella, C. V. Falub, T. Kreiliger, M. Salvalaglio, R. Bergamaschini, E. Grilli, M. Guzzi, H. von Känel, and L. Miglio, Ge crystals on Si show their light, *Phys. Rev. Appl.* **1**, 044005 (2014).
- [47] F. Pezzoli, A. Giorgioni, K. Gallacher, F. Isa, P. Biagioni, R. W. Millar, E. Gatti, E. Grilli, E. Bonera, G. Isella, D. J. Paul, and L. Miglio, Disentangling nonradiative recombination processes in Ge micro-crystals on Si substrates, *Appl. Phys. Lett.* **108**, 262103 (2016).
- [48] M. A. Reshchikov, Temperature dependence of defect-related photoluminescence in III-V and II-VI semiconductors, *J. Appl. Phys.* **115**, 012010 (2014).
- [49] E. F. Schubert, *Light-Emitting Diodes* (Cambridge University Press, Cambridge, UK, 2006), Chap. 2.
- [50] W. Shockley and W. T. Read, Statistics of the recombinations of holes and electrons, *Phys. Rev.* **87**, 835 (1952).
- [51] R. N. Hall, Electron-hole recombination in germanium, *Phys. Rev.* **87**, 387 (1952).
- [52] M. I. Dyakonov and V. I. Perel, *Optical Orientation* (North-Holland, New York, 1984), Chap. 2.
- [53] G. Lampel, Nuclear Dynamic Polarization by Optical Electronic Saturation and Optical Pumping in Semiconductors, *Phys. Rev. Lett.* **20**, 491 (1968).
- [54] I. Žutić, J. Fabian, and S. Das Sarma, Spintronics: Fundamentals and applications, *Rev. Mod. Phys.* **76**, 323 (2004).
- [55] J. Rioux and J. E. Sipe, Optical injection and control in germanium: Thirty-band  $k \cdot p$  theory, *Phys. Rev. B* **81**, 155215 (2010).
- [56] E. J. Loren, J. Rioux, C. Lange, J. E. Sipe, H. M. van Driel, and A. L. Smirl, Hole spin relaxation and intervalley electron scattering in germanium, *Phys. Rev. B* **84**, 214307 (2011).
- [57] C. Lange, G. Isella, D. Chrastina, F. Pezzoli, N. S. Köster, R. Woscholski, and S. Chatterjee, Spin band-gap renormalization and hole spin dynamics in Ge/SiGe quantum wells, *Phys. Rev. B* **85**, 241303(R) (2012).
- [58] K. Zerrouati, F. Fabre, G. Bacquet, J. Bandet, J. Frandon, G. Lampel, and D. Paget, Spin-lattice relaxation in  $p$ -type gallium arsenide single crystals, *Phys. Rev. B* **37**, 1334 (1988).
- [59] Y. Song, O. Chalaev, and H. Dery, Donor-Driven Spin Relaxation in Multivalley Semiconductors, *Phys. Rev. Lett.* **113**, 167201 (2014).
- [60] J.-M. Tang, B. T. Collins, and M. E. Flatté, Electron spin-phonon interaction symmetries and tunable spin relaxation in silicon and germanium, *Phys. Rev. B* **85**, 045202 (2012).
- [61] G. Lancaster, J. A. Van Wyk, and E. E. Schneider, Spin-lattice relaxation of conduction electrons in silicon, *Proc. Phys. Soc.* **84**, 19 (1964).
- [62] J. L. Cheng, M. W. Wu, and J. Fabian, Theory of the Spin Relaxation of Conduction Electrons in Silicon, *Phys. Rev. Lett.* **104**, 016601 (2010).
- [63] F. Rortais, C. Vergnaud, A. Marty, L. Vila, J.-P. Attané, J. Widiez, C. Zucchetti, F. Bottegoni, H. Jaffrès, J.-M. George, and M. Jamet, Non-local electrical spin injection and detection in germanium at room temperature, *Appl. Phys. Lett.* **111**, 182401 (2017).
- [64] A. Jain, J.-C. Rojas-Sanchez, M. Cubukcu, J. Peiro, J. C. Le Breton, E. Prestat, C. Vergnaud, L. Louahadj, C. Portemont, C. Ducruet, V. Baltz, A. Barski, P. Bayle-Guillemaud, L. Vila, J.-P. Attané, E. Augendre, G. Desfonds, S. Gambarelli, H. Jaffrès, J.-M. George, and M. Jamet, Crossover from Spin Accumulation into Interface States to Spin Injection in the Germanium Conduction Band, *Phys. Rev. Lett.* **109**, 106603 (2012).
- [65] M. Yamada, M. Tsukahara, Y. Fujita, T. Naito, S. Yamada, K. Sawano, and K. Hamaya, Room-temperature spin transport in N-Ge probed by four-terminal nonlocal measurements, *Appl. Phys. Express* **10**, 093001 (2017).
- [66] A. Malinowski, R. S. Britton, T. Grevatt, R. T. Harley, D. A. Ritchie, and M. Y. Simmons, Spin relaxation in GaAs/ $\text{Al}_x\text{Ga}_{1-x}\text{As}$  quantum wells, *Phys. Rev. B* **62**, 13034 (2000).
- [67] S. G. Bhat and P. S. A. Kumar, Room temperature electrical spin injection into GaAs by an oxide spin injector, *Sci. Rep.* **4**, 5588 (2014).
- [68] C. Hautmann and M. Betz, Magneto-optical analysis of the effective  $g$  tensor and electron spin decoherence in the multivalley conduction band of bulk germanium, *Phys. Rev. B* **85**, 121203 (2012).
- [69] A. D. Margulis and V. I. Margulis, Spin relaxation of conduction electrons in semiconductors in a strong magnetic field. The precession mechanism, *Fiz. Tverd. Tela* **25**, 1590 (1983) [*Sov. Phys. Solid State* **25**, 918 (1983)].
- [70] V. V. Belykh, A. Greulich, D. R. Yakovlev, M. Yacob, J. P. Reithmaier, M. Benyoucef, and M. Bayer, Electron and hole  $g$  factors in InAs/InAlGaAs self-assembled quantum dots emitting at telecom wavelengths, *Phys. Rev. B* **92**, 165307 (2015).